The Free Energy Cost of Interdigitation of Lamellar

Bilayers of Fatty Alcohols with Cationic Surfactants

from Molecular Dynamics Simulations

Futianyi Wang and Ronald G. Larson^{*}

Department of Chemical Engineering, University of Michigan, Ann Arbor, Michigan, 48105

*Corresponding Author: Tel. 1-734-936-0772

E-mail address: <u>rlarson@umich.edu</u>

Electronic supplementary information (ESI) available

Abstract

Cationic surfactant mixed with fatty alcohol as co-surfactant in excess water can form

stable emulsions, known as "lamellar gel networks," that contain extended and interconnected

networks of swollen bilayers, including ones with in-plane liquid-like disorder (L_{α} phase) and

solid-like order (L_{B} phase). To study their structure and thermodynamics, molecular dynamics

(MD) simulations with lateral pressure and temperature scans along reversible pathways were used

to drive reversible phase changes, including formation at negative lateral pressure of the L_{BI} phase

with interdigitated tails of opposing leaflets. Thermodynamic integration, with extrapolations to

infinitely slow scans, yielded a free energy difference between the interdigitated $L_{\beta I}$ and non-

interdigitated L_B phase of 2.4 ± 0.5 kJ/mol, which is consistent with the spontaneous formation of

 L_{β} phase under atmospheric pressure in simulation. Thermodynamic cycles involving temperature

and lateral pressure for which the free energy difference is identically zero were constructed as

1

negative controls to verify the method. Using lateral pressure, including negative lateral pressure, helps avoid kinetic bottlenecks that occur when temperature alone is used as the control variable. The method, using negative lateral pressure, should be widely applicable to other bilayers to identify molecular properties that control interdigitation and other bilayer properties.

1. Introduction

Surfactants that lower the surface tension between oil and water are usually amphiphilic organic compounds with hydrophobic tail groups and hydrophilic head groups, which can be either ionic or non-ionic. In the bulk aqueous phase, surfactants can aggregate into micelles with the aggregate core formed by the hydrophobic tails and the hydrophilic heads in contact with surrounding water. Other types of aggregate structure can also be formed such as spherical or cylindrical micelles or bilayers, depending on surfactant concentration and its chemical structure. Fatty alcohols are also amphiphilic molecules with a polar hydroxyl head associated attached to an alkyl chain tail. Long-chain alcohols such as cetyl (C16) and stearyl (C18) alcohols are only weak emulsifiers by themselves and adopt various crystalline structures with poor hydration capacity in water. However, when they are mixed with surfactants in an appropriate ratio in excess water, stable emulsion can form, which are widely used in pharmaceutical creams, cosmetic lotions, hair care products and as drug delivery carriers with other essential additives such as salt and perfume.²³ Hair conditioner has been a particularly important product application for these emulsions in the hair and skin-care industry due to the enormous market demand for such products over the past few decades. The cationic surfactant in the conditioner adheres well to the slightly negatively charged wet hair, while the fatty alcohol component helps in lubricating and moisturizing the hair surface to provide a smooth feel.

These pseudo-ternary mixtures contain extended and highly interconnected networks often referred as "lamellar gel networks," which can withstand elastic deformation and have interesting rheological properties. As a result of the multiphase structure, lamellar gel networks of surfactant and fatty alcohol have an opaque creamy appearance and exhibit highly viscous, shear-thinning rheology.56 The basic units of the networks are highly swollen bilayers self-assembled from surfactant and fatty alcohol molecules with regular in-plane spacing, and inter-lamellar regions filled with water. The swelling of the lamellar stacks by water is caused by steric or electrostatic repulsion of the surfactant head groups which produces an osmotic pressure in the hydrophilic region of the lamellae. The bilayers in lamellar gel networks can form different phases depending on their composition and temperature, similar to other bilayer systems such as lipid membranes. At low temperature, the bilayers form a stiff, gel phase known as the L_{β} phase, where the C-C bonds in the hydrocarbon chains adopt all-trans conformations and the molecules are tightly packed in hexagonal order within each leaflet. Upon increase of temperature, gauche conformations take over and the bilayer melts into a more fluidic, liquid crystalline L_{α} phase with loosely packed hydrocarbon chains and shortened extension. Several other structures have been reported for the gel phase, such as an $L_{\beta I}$ phase with an interdigitated bilayer and an L_{β} , phase with molecules tilted with respect to the bilayer normal. In the interdigitated gel phase (L_{BI}), the hydrocarbon chains interpenetrate to maximize van der Waals interactions and reduce head group crowding at the expense of unfavorable exposure to the surrounding aqueous solution.¹²

Despite the wide application of lamellar gel networks, their flow properties and microstructures and how these are controlled at the molecular level remain relatively mysterious. In particular, whether those bilayers are interdigitated or not, and what controls this property, is as yet not well understood. In addition to rheology characterization, small-angle X-ray scattering

(SAXS) and X-ray diffraction have been used to investigate the structure of lamellar bilayers. Other experimental approaches such as Fourier-transform infrared spectroscopy (FTIR), NMR and differential scanning calorimetry (DSC) have also been applied to study the phase transitions of other systems such as lipid bilayers. While these experimental studies have produced valuable insight into understanding bilayer structure, the majority of them yield only one-dimensional information mostly along the bilayer normal, namely inter-lamellar spacings and thickness of bilayers. In contrast, computer simulations have emerged as an attractive technique to obtain microscopic three-dimensional structural information of bilayers. The models employed in simulations range from fully atomistic models to coarse-grained bead-spring descriptions. With calibrated force-field parameters, molecular dynamics (MD) simulations can play an important role in investigating bilayer properties and their dependences on the composition and molecular structure of the constituents, and their molecular level interactions.

Although there are extensive MD simulation studies on lipid bilayers and surfactant micelles, there is limited information on mixed surfactant systems and on bilayer interdigitation, especially from all-atom simulations. Shigematsu et al. investigated stretched-induced interdigitation of a phospholipid/cholesterol bilayer with united-atom MD simulations and proposed a free energy model. Laner et al. used united-atom models to study methanol-induced interdigitation of glycerol-monopalmitate lipid bilayers and found that while the simulation starting structure could affect the final structure formed, no direct transition from $L_{\beta I}$ to L_{β} phase was observed. The final structure dissipative particle dynamics (DPD) simulation. With DPD simulation, Lu and Guo demonstrated the phase behavior of lipid bilayers including an interdigitated gel phase. In a recent study, Seo et al. revealed how interdigitated acyl chains

modulated the partitioning of cholesterol in the opposing leaflet and affected the phase behavior of an asymmetric lipid membrane with coarse-grained MD simulation.²¹ For a mixture of cationic surfactant and fatty alcohol present in lamellar gel networks, Debnath et al. used united-atom simulations to investigate the effect of bilayer composition and water concentration on the phase transition on non-interdigitated and interdigitated bilayers in separate publications, leaving some confusion as to which one is the equilibrium structure.²² In addition, Leonforte et al. were able to simulate with an all-atom forcefield the gel-fluid bilayer transition of a similar surfactant/fatty alcohol mixture.²³ Because of the limited time and length scales accessible with all-atom MD simulations, kinetic trapping is oftentimes an issue especially at low temperature, which prevents the formation of the equilibrium structure of these bilayer systems in the gel state. Thus, although insights are gained from simulations such as these, conclusive evidence determining whether interdigitation is thermodynamically favored or not for a given model forcefield, is still lacking.

Comparing the free energies of the L_{β} and $L_{\beta I}$ phases might determine which of them is the equilibrium state, but the lack of a smooth transition route between the two phases has prevented us, despite numerous efforts, from calculating the free energy difference with methods such as umbrella sampling, where the degree of interdigitation is the reaction coordinate. In this paper, we show that lateral pressure as a second parameter besides temperature allows the creation of reversible pathways to connect L_{β} and $L_{\beta I}$ phase. Based on this discovery, we propose a method to calculate the free energy cost of bilayer interdigitation using thermodynamic integration.

2. Theory

Let us first consider the bilayer system composed of fatty alcohol and cationic surfactant in the L_{β} phase at room temperature and atmospheric pressure. As illustrated on the right side of

Figure 1, when the simulated L_{β} phase (lower right corner) was gradually heated at constant pressure (1 bar), the bilayer turned into an L_{α} phase (upper right corner) at high temperature as expected. The bilayer in the fluidic L_{α} phase could be stretched by imposing a negative lateral pressure on the system, as shown on the upper half of Figure 1. With the bilayer in the stretched state with decreased thickness and increased apparent bilayer area, the spontaneous formation of an interdigitated bilayer in LBI phase occurred when the system was cooled back to room temperature while maintaining the negative lateral pressure, as shown by the two images on the left side of Figure 1. Finally, changing the lateral pressure back to atmospheric pressure led to a bilayer at the same starting temperature and pressure as in the lower right-hand corner of Figure 1, but in the L_{BI} phase instead of the initial L_{B} phase. The above transitions were found to be "reversible" in the sense that the states at either end of the transition could be recovered one from the other traversing the transition in either direction by varying the system temperature at fixed pressure or the lateral pressure at fixed temperature. This contrasts with the lack of a spontaneous, direct, transition between the L_{β} and $L_{\beta I}$ phase, both of which remained stable during runs at atmospheric pressure and room temperature. We indicate this in Figure 1 by an "X" over this transition, showing that both states are metastable at atmospheric conditions, although only one of them is the thermodynamically stable state. However, it is theoretically possible to calculate the free energy change along the indirect pathways by thermodynamic integration.

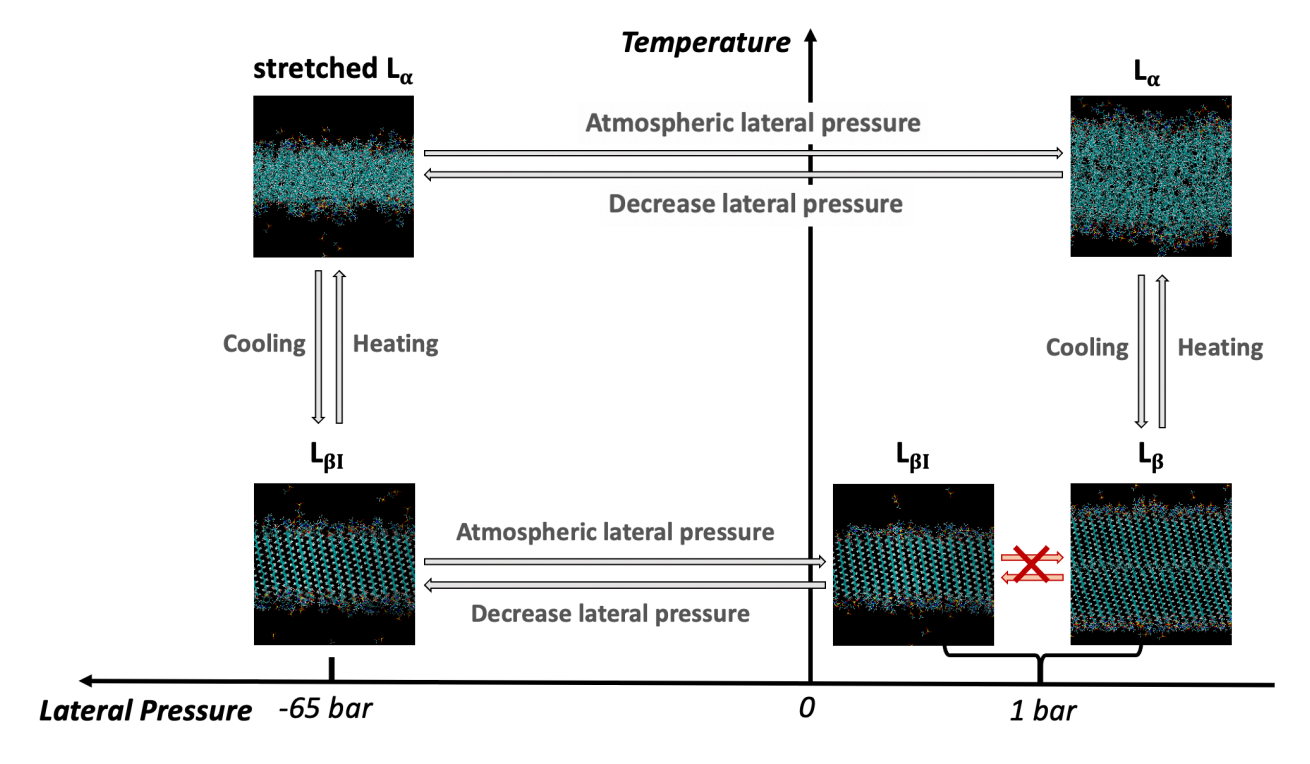


Figure 1. Snapshots of different bilayer phases upon changes of temperature or lateral pressure in the x and y directions. The pressure in the z direction perpendicular to the bilayer remains at atmospheric pressure. Water molecules are hidden.

Here, we consider the Helmholtz free energy of F of the system, which is defined as the internal energy U plus the product of temperature T and entropy S. The change of internal energy dU equals the change of heat and work done and can be written as TdS - pdV for a reversible change. (Here we take the pressure to be isotropic for simplicity, but below we generalize to allow for anisotropic pressure, in which lateral pressure in the plane of the bilayer differs from transverse pressure perpendicular to it.) The change of free energy dF is equal to -SdT - pdV in differential form. As the system volume changes reversibly with varying pressure in continuous small steps at constant temperature, the change of free energy ΔF can be calculated from the integral of -pdV as follows:

$$F \equiv U - TS \tag{1}$$

$$dU = T dS - p dV = d(TS) - S dT - p dV$$
 (2)

$$dF = dU - d(TS) = -S dT - p dV$$
 (3)

$$\Rightarrow \Delta F = -\int p \, dV \, for \, constant \, T \tag{4}$$

On the other hand, the average internal energy U and the thermal average of a generalized force X corresponding to an external displacement variable x can be expressed in terms of the canonical partition function Z and $\beta = \frac{1}{kT}$ to give the differential form of $\log Z$. The Helmholtz free energy is also related to the canonical partition function as $F = -\frac{\log Z}{\beta}$. As shown in the following derivation, the change of the ratio of free energy to temperature, $\Delta\left(\frac{F}{T}\right)$, can be written as the integral of the internal energy U over the inverse of temperature $d\left(\frac{1}{T}\right)$ plus the integral of a generalized force X divided by temperature T over the external variable dx. Statistical thermodynamics gives the following two identities:

$$U \equiv \langle E \rangle = -\frac{\partial \log Z}{\partial \beta} \tag{5}$$

$$X = \frac{1}{\beta} \frac{\partial \log Z}{\partial x} \tag{6}$$

where the derivative with respect to β is taken at fixed x, and that with respect to x is at fixed β . All logarithms are natural logs. We can then obtain from these

$$d(\log Z) = -U d\beta + \beta X dx \tag{7}$$

We also have the identity:

$$F = -\frac{\log Z}{\beta} \tag{8}$$

which, when combined with the previous equation of $d(\log Z)$, gives

$$d(F\beta) = d(-\log Z) = U d\beta - \beta X dx \tag{9}$$

Using the definition of $\beta = \frac{1}{kT}$,

$$d\left(\frac{F}{T}\right) = U d\left(\frac{1}{T}\right) - \frac{X}{T} dx \tag{10}$$

which leads to the desired result:

$$\Delta\left(\frac{F}{T}\right) = \int U \, d\left(\frac{1}{T}\right) - \int \frac{X}{T} \, dx \tag{11}$$

The generalized force X in each direction can be calculated from the anisotropic pressures time the area on each side of the simulation box while the displacement dx is just the change of simulation box dimensions. The total energy and temperature are also recorded during simulations. Therefore, the free energy change resulting from varying temperature at constant pressure can be evaluated as well. Based on the above thermodynamic principles, the free energy change can be calculated for two systems starting in same structure (L_{α}) at high temperature and atmospheric pressure after passing through different reversible pathways taking them into two different structures (L_{β} and $L_{\beta I}$) at the same low temperature and atmospheric pressure. As shown in Figure 2, since the starting states are exactly the same and the final states are also at the same temperature and pressure and the pathways are reversible, the difference in free energy change along the two pathways is equal to the free energy difference of their final states, which here are the interdigitated ($L_{\beta I}$) and non- interdigitated bilayer (L_{β}).

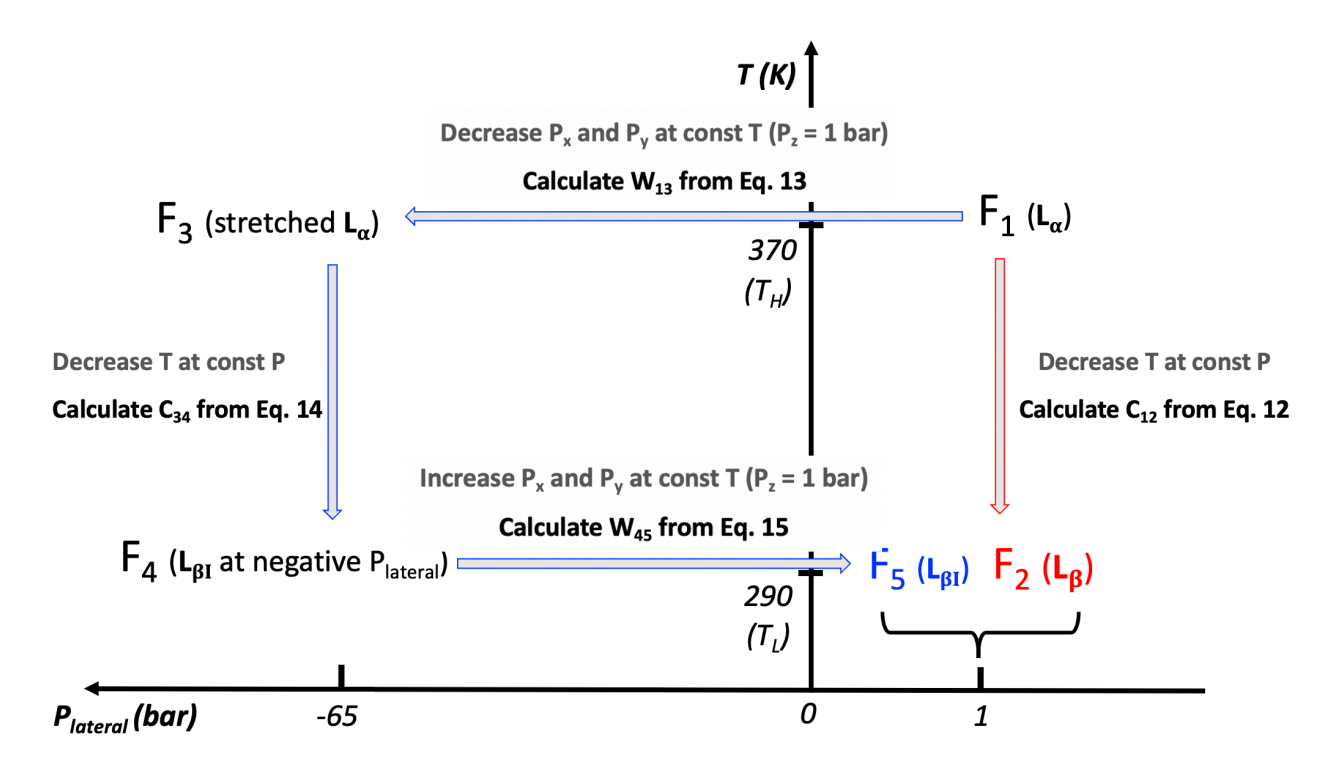


Figure 2. Two thermodynamic pathways from the same starting state: F₁, to two different final states, namely, F₂: the non-interdigitated bilayer formed via the red pathway, and F₃: the interdigitated bilayer formed via the blue pathway. Both pathways are at 290 K and atmospheric pressure.

The following four equations (Eqs. 12-15) are derived from the above scheme to relate the unknown free energies of five different states (F_1 to F_2) to quantities (C_1 , W_2 , C_3 , and W_4) that can be calculated from simulation by thermodynamic integration. The anisotropic pressures are P_2 , P_2 , and P_2 and P_3 and P_4 are the simulation box dimensions. After rearrangement, the free energy difference between P_3 and P_4 and P_5 and P_6 are the simulation box dimensions.

$$\frac{F_2}{T_L} - \frac{F_1}{T_H} = \Delta \left(\frac{F}{T}\right) = \int U \, d\left(\frac{1}{T}\right) - \int \frac{P_x L_x L_y \, dL_z + P_y L_x L_z \, dL_y + P_z L_x L_y \, dL_z}{T} = C_{12} \tag{12}$$

$$F_3 - F_1 = \Delta F = -\int P \, dV = \int P_x L_x L_y \, dL_z + P_y L_x L_z \, dL_y + P_z L_x L_y \, dL_z = W_{13}$$
 (13)

$$\frac{F_4}{T_L} - \frac{F_3}{T_H} = \Delta \left(\frac{F}{T}\right) = \int U \, d\left(\frac{1}{T}\right) - \int \frac{P_x L_x L_y \, dL_z + P_y L_x L_z \, dL_y + P_z L_x L_y \, dL_z}{T} = C_{34} \qquad (14)$$

$$F_5 - F_4 = \Delta F = -\int P \ dV = \int P_x L_x L_y \ dL_z + P_y L_x L_z \ dL_y + P_z L_x L_y \ dL_z = W_{45}$$
 (15)

$$F_5 - F_2 = W_{45} + T_L \left[C_{34} - C_{12} + \frac{W_{13}}{T_H} \right]$$
 (16)

While Eqs. 12-16 apply for general displacements in three dimensions, we restrict our interest to lateral pressure change with semiisotropic pressure coupling in which $dL_x = dL_y$, $P_x = P_y$, and P_z stays at a constant of 1 bar.

3. Molecular Dynamics Simulation Methods

Bilayer composition, and simulation details

All-atom MD simulations were carried out for bilayers consisting of the cationic surfactant (CS) behentrimonium methylsulfate (BTMS) and the fatty alcohol (FA) stearyl alcohol (C_n) as the fatty alcohol (FA) cosurfactant. The simulation system consisted of 46 BTMS, 154 stearyl alcohol to match the CS:FA molar ratio in the experimental sample for rheology characterization and 12000 water molecules. The simulation system has 77 wt% of water, which is reduced from the 93 wt% in the actual industrial application due to the limitation on system size, but the mixed surfactant bilayers are still sufficiently hydrated with large enough lamellar spacing that the water content is not expected to influence the phase transitions. The surfactant and fatty alcohol molecules were packed into the bilayer to create the initial configuration, and then equilibrated at 290 K for at least 40 ns to obtain the gel state structure. The forcefield parameters were adopted from L-OPLS with the rigid SPC/E model for water. For NPT simulations, a time step of 1 fs was used. The temperatures of cationic surfactant, fatty alcohol and water were separately controlled by the velocity-rescale coupling method with a time constant of 0.1 ps. Pressure was controlled by the Parrinello-Rahman semi-isotropic coupling method with a time constant of 2.0

ps, which allows the lateral pressure in x and y direction and the pressure in z direction to be set differently.²⁸ A Verlet neighbor-searching scheme was used and both Coulombic and van der Waals interactions were cut off at 1.2 nm. Long range electrostatic interactions were treated using the particle-mesh Ewald method with an interpolation order of 4 and 0.12 nm Fourier spacing.²⁹ Periodic boundary conditions were applied in all three directions. System energy, temperature and periodic box dimensions were saved every 10 ps, with results reported here being insensitive to this choice. All simulations were performed with GROMACS 2019.^{20,31}

Variations of temperature and lateral pressure

To control the phase transition, a linear temperature ramp from 290 K to 370 K was imposed with various heating/cooling rates ranging from 2.0 K/ns to 0.25 K/ns. The actual temperature fluctuated somewhat from this linear ramp on short time scales, so that the increase was not strictly monotonic. Therefore, the recorded temperatures and the corresponding total energies were reordered before integrating the total energy over the inverse of temperature. Since pressure could not be changed during a simulation run, separate simulation runs at different lateral pressures were performed to approximate a continuously changing pressure using linear interpolation. The lateral pressure was varied from 1 bar to -65 bar with an interval of 10 bar, each for 20 ns to allow the system to reach equilibrium, and a subsequent 20 ns of sampling to calculate average properties.

Monitoring phase transitions

To monitor structural change in the bilayer, the carbon-hydrogen order parameter of the alkyl chains in the molecules is computed for each carbon along the alkyl chain:

$$S_{CD} = \frac{1}{2} |3\cos^2\theta - 1| \tag{17}$$

where θ is the angle between the C-H bond vector and the bilayer normal. This order parameter is averaged over all the carbons of all alkyl chains and used to identify the phase transition of the bilayer, supported by snapshots from the simulation.

4. Results and Discussion

Phase transitions

Bilayers with separate leaflets were built as the initial structure and assembled into a bilayer. When the system was equilibrated at 290 K and 1 bar, the bilayer formed a tilted L_{β} phase shown in the lower right-hand corner of Figure 1 with the alkyl chains hexagonally packed in each leaflet shown in Figure 3a. As the temperature was increased, at above 355 K the bilayer melted as expected into an L_{α} phase with much lower order parameter shown in the upper right-hand corner of Figure 1. The packing of alkyl chains in the leaflets also loses the hexagonal order as shown in Figure 3b. The melting temperature from the simulation is reasonably close to the values of around 340-350 K reported in previous simulations and differential calorimetry (DSC) experimental data of similar systems. The L_{β} to L_{α} phase change is reversed upon cooling, although at a lower transition temperature due to hysteresis.

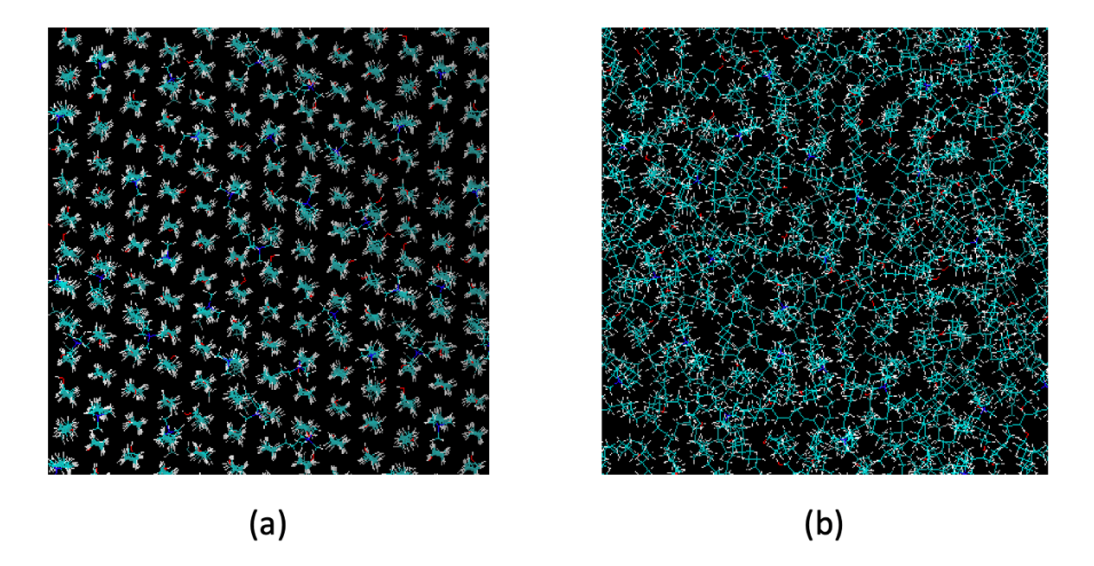


Figure 3. Packing of FA and CS in one leaflet of the bilayer in (a) L_{β} phase (hexagonal order), and (b) L_{α} phase (disorder).

To investigate the formation of the interdigitated $L_{\beta I}$ phase, a negative lateral pressure in the x and y directions was applied to stretch the L_{α} bilayer at 370 K into a thinner state with the two leaflets penetrating more into each other as shown in the upper half of Figure 1. The average area per molecule in the leaflet increases by 76% from 0.307 nm² to 0.540 nm² at -65 bar in Figure 4. The order parameter S_{co} also further decreased from 0.15 of the unstretched state to 0.05 of the stretched state, which can be seen by comparing the endpoints on Figure 6a and 6b. The deformation of the bilayer was reversible when the lateral pressure was changed back to 1 bar. Successive cooling of the stretched L_{α} bilayer at negative lateral pressure could lead to the spontaneous formation of an ordered, interdigitated $L_{\beta I}$ phase as shown on the left side of Figure 1. Afterwards, heating the bilayer in the interdigitated $L_{\beta I}$ phase under negative lateral pressure could bring the bilayer back into the stretched L_{α} phase. However, a critical lateral pressure between -40 and -50 bar was required for sufficient deformation to induce enough interdigitation.

Otherwise, a less stretched L_{α} bilayer would turn into the non-interdigitated L_{β} phase upon cooling as shown by the comparison in Figure S1. The surface tension on the bilayer caused by the stretching is also plotted in Figure 5, which shows that that the critical tension value required for the formation of the interdigitated bilayer is around 5 x 10° N/m. We note that an equivalent way of computing free energy is to control surface tension, rather than lateral pressure. While no pore formation was observed during the bilayer stretching presented in this work, the fluidic L_{α} bilayer could be prone to rupture if much higher tension is imposed.

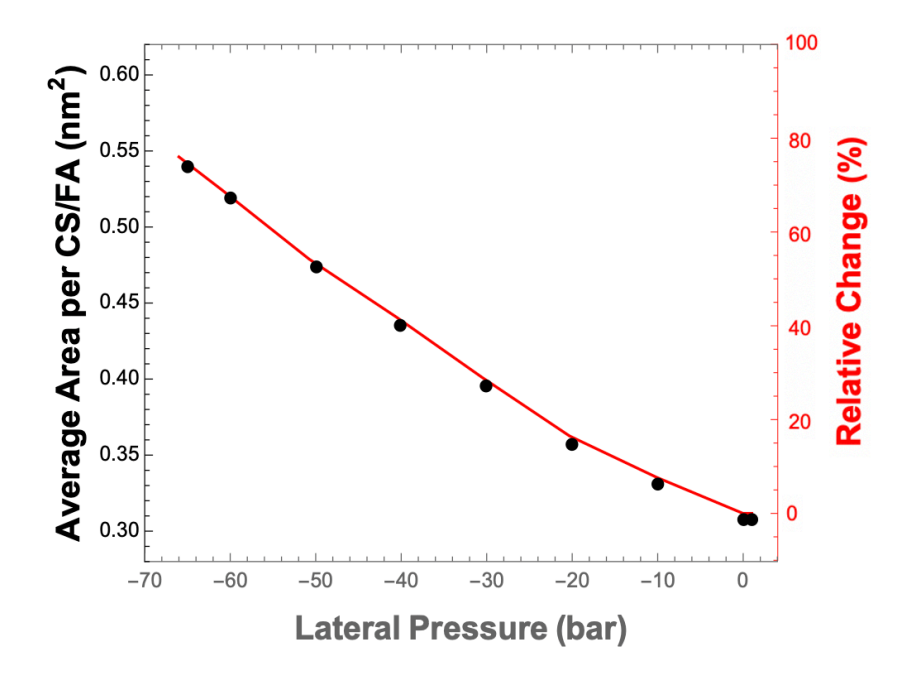


Figure 4. Change of average area per CS/FA molecules in each leaflet when the bilayer in the L_{α} phase is stretched under different negative lateral pressures, in a sequence from right to left from 1 to -65 bar.

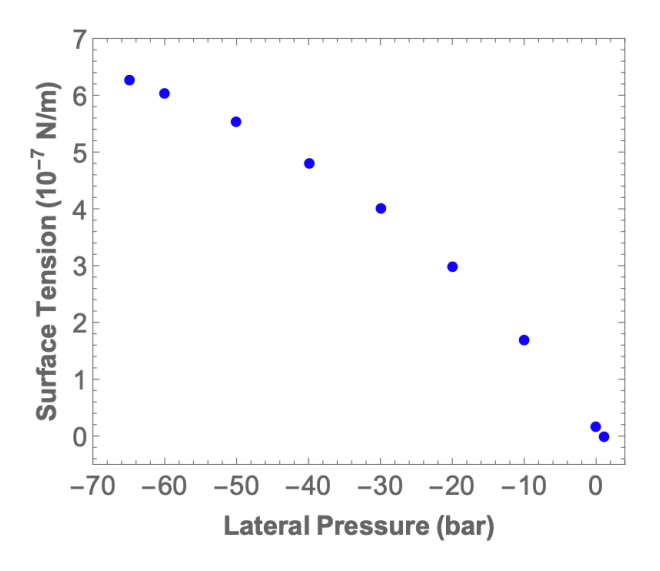


Figure 5. Dependance of surface tension on the bilayer to lateral pressure, varied from right to left from 1 to -65 bar.

Thermodynamic integration

With the method proposed, we calculate C_n and C_n during the temperature change at each of the two fixed pressures and W_n and W_n and W_n and W_n are equal to the PV work done if the pressure change is carried out in small steps and the volume change is reversible. In practice, W_n and W_n were approximated by numerical integration of the PV change and interpolation from a series of simulations at 370 K and 290 K with different lateral pressures. The bilayer in the L_{α} phase gradually expanded laterally in the x and y directions and shrank in the z direction when the lateral pressure changed from 1 bar to -65 bar with P, fixed at 1 bar as shown in Figure S7. Since the absolute value of the lateral pressure was much larger than P, and the system was expanding against a negative lateral pressure, the free energy increased during the bilayer stretching giving $W_n = 3.45$ kJ/mol, a positive value. In contrast, W_n corresponds to a lateral pressure change from -65 bar back to 1 bar on the bilayer system in the rigid $L_{\beta I}$ phase with much less volume change, thus giving a negative and much smaller absolute free energy change, $W_n = -0.40$ kJ/mol.

The calculation of C_{12} and C_{34} by numerical integration of the system energy over increments of inverse temperature is subjective to uncertainties due to hysteresis between cooling and heating. Hysteresis is revealed by a difference in the transition temperature between the high temperature L_{α} phase and either the L_{β} or the $L_{\beta 1}$ phase upon heating vs. cooling. To investigate the hysteresis effect, both the interdigitated and non-interdigitated system were heated from 290 K to 370 K and cooled from 370 K to 290 K at different rate of change of temperature. As shown in plots of the order parameter in Figure 6, hysteresis is more significant for cooling especially for the interdigitated bilayer and decreases with slower heating or cooling rates.

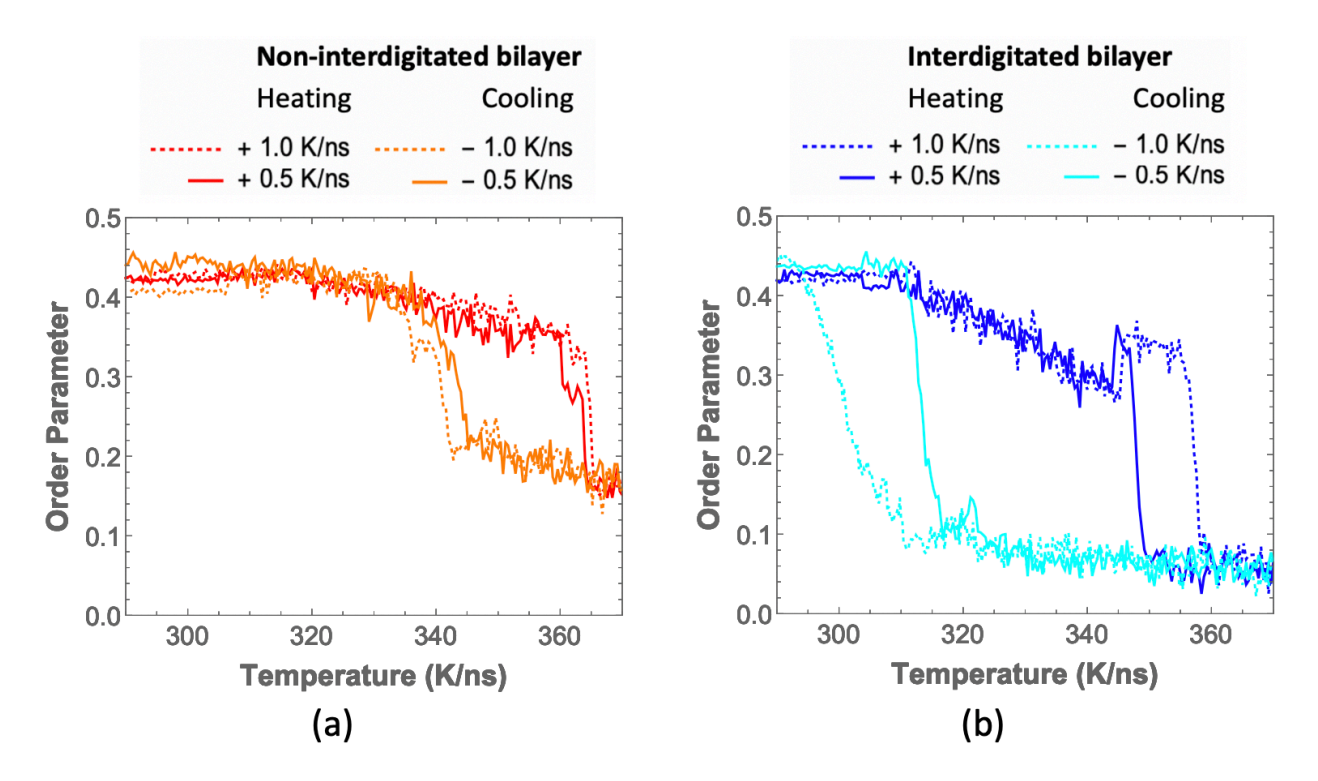


Figure 6. Hysteresis in change of average order parameter S_{ω} (calculated from Eq. 17) of the fatty alcohol molecules during heating and cooling at two different rates for (a) transition of non-interdigitated bilayer system between L_{α} and L_{β} phases at atmospheric pressure, (b) transition of interdigitated bilayer system between stretched L_{α} and $L_{\beta l}$ phases at -65 bar lateral pressure.

In theory, hysteresis will be eliminated if the rate of temperature change is made infinitely small, but it remains finite with any finite simulation time. To extrapolate towards infinitely slow rate, we plot in Figure 7 C_n (corresponding to a phase transition in a non-interdigitated bilayer) and C_n (corresponding to a phase transition of in an interdigitated bilayer under negative lateral pressure) calculated from simulations of heating or cooling at different rates. Ideally, the data points from heating and cooling simulations should converge when extrapolated to an infinitely slow rate of temperature change. For both systems, the data points from heating and cooling do approach each other as the rate of temperature change decreases, and those from heating are less sensitive to the change of heating rate and fit better to a linear extrapolation than do those from cooling. This is not surprising, since melting is faster than crystallization and not as susceptible to defect formation. Therefore, data points from the heating simulation should be the more reliable data and were therefore used for our free energy calculations. The extrapolated values of the constants obtained from the four thermodynamic integrations shown in Figure 2 are given in the row of values labeled "L_{BI} vs L_B" in Table 1.

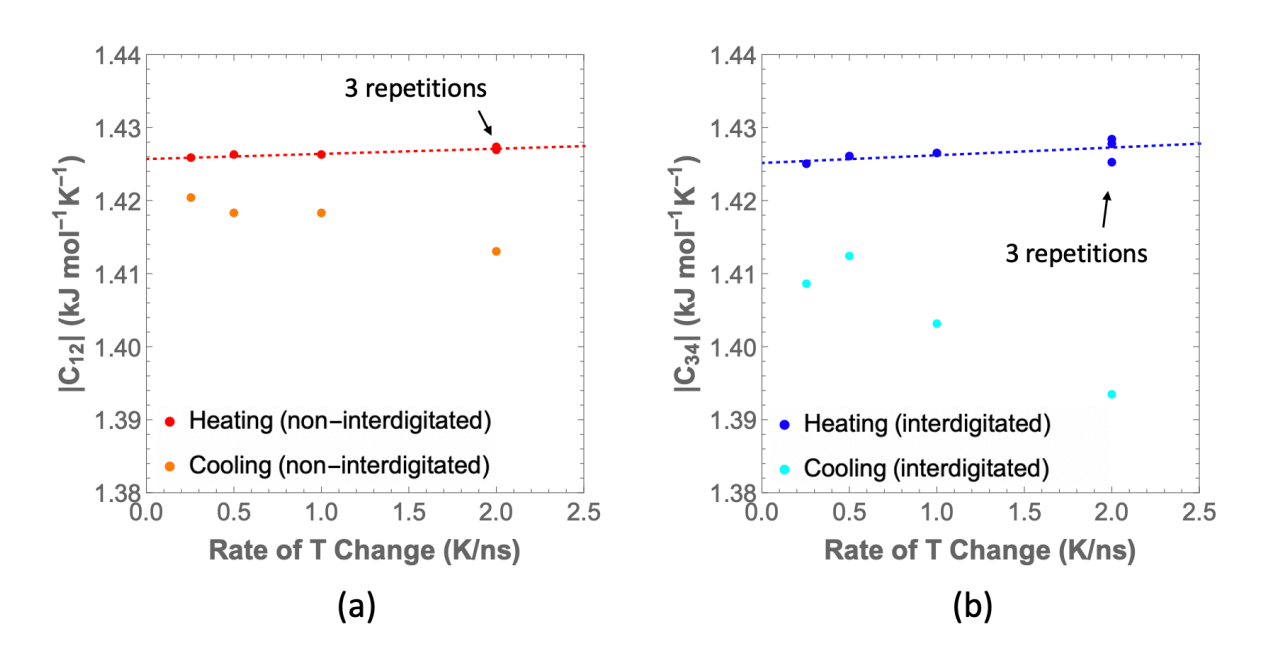


Figure 7. Effect of hysteresis on value of (a) C₁ for non-interdigitated bilayer, and (b) C₂ for interdigitated bilayer.

To investigate the potential influence of the lateral density distribution of the two components, bilayers with more homogenously dispersed cationic surfactant molecules were created as shown in Figure 8b. No significant difference was found in the phase transition temperature or in results from thermodynamic integration (Figure S2). Since a perfectly "homogenous" bilayer almost never spontaneously forms by cooling of the \boldsymbol{L}_{α} phase in the simulation, bilayers with randomly dispersed cationic surfactants were used in the simulations in the main text. In addition, a smaller simulation system with 36 molecules in each bilayer leaflet instead of the 100 of the original system with almost the same CS:FA ratio (8 CS and 28 FA) and water content was created to investigate the influence of system size. Heating simulations at 2.0 K/ns and 0.5 K/ns were performed for both the interdigitated bilayer and the non-interdigitated bilayer. The values of C₁₂ and C₃₄ calculated from the smaller system are very close to the ones from the original system (Figure S3), proving that the result is not affected by system size. The test with different system size also addresses the concern with non-zero off-diagonal pressure tensors, especially the xy stress distortions. At 290 K, the xy stress is around 2 bar for L_{β} phase at 1 bar lateral pressure and 19 bar for $L_{\beta I}$ phase at -65 bar lateral pressure, which is caused by the boxinduced distortion of the hexagonal phase, and this stress vanishes when the bilayer turns into an L_{α} phase at high temperature. Since non-zero shear stresses will get smaller for bigger systems, the fact that both systems give similar results indicates that the bias in pressure does not change the main results of the paper.

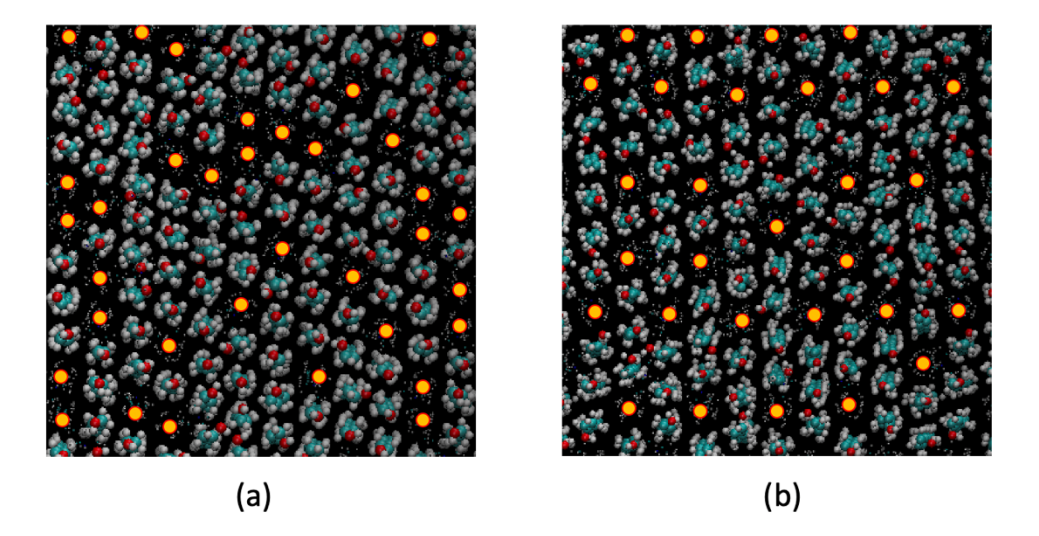


Figure 8. Lateral distribution of FA and CS hexagonally packed in one leaflet of the bilayer in L_{β} phase: (a) with random dispersion of CS, (b) with artificially created more homogenous dispersion of CS. CS molecules are highlighted with orange circles.

Based on the proposed method, the free energy difference between $L_{\beta I}$ and L_{β} phases at 290 K, and atmospheric pressure, was calculated to be 2.4 kJ/mol of surfactant and fatty alcohol. The major source of error comes from the extrapolation of C_{12} and C_{34} from linear regression, where the 95% confidence interval produces an uncertainty of \pm 0.5 kJ/mol. The positive free energy difference indicates that the bilayer with an L_{β} structure has the lower free energy and is more stable. The result agrees with the spontaneous formation of non-interdigitated bilayer observed in simulation.

Verification with thermodynamic cycles

To further verify the proposed method, two thermodynamic cycles were constructed, one for a non-interdigitated bilayer and the other for an interdigitated bilayer at different negative lateral pressures as illustrated in Figure 9. In the previous case, a difference in free energy change resulted from the two pathways from the same starting state, since the pathways led to two different

final states, namely L_{β} and $L_{\beta I}$ phases. In the two new cycles presented in Figure 9, the same starting states transition to the same final states via two different pathways and therefore the theoretical difference between the two pathways of each system should be zero. The same method as used above was also used for free energy calculations in heating simulations, although the extrapolation of $C_{\text{\tiny SI}}$ was based on three different heating rates instead of four (Figure S4). The two cycles in Figure 9 (a) and (b) converged with errors of 0.3 and 0.4 kJ/mol respectively from Table 1, which is within the estimated systematic error. These simulations indicate that our method of computing free energy differences between namely $L_{\beta I}$ and L_{β} phases using these thermodynamic cycles is valid and has error well below the calculated free energy difference.

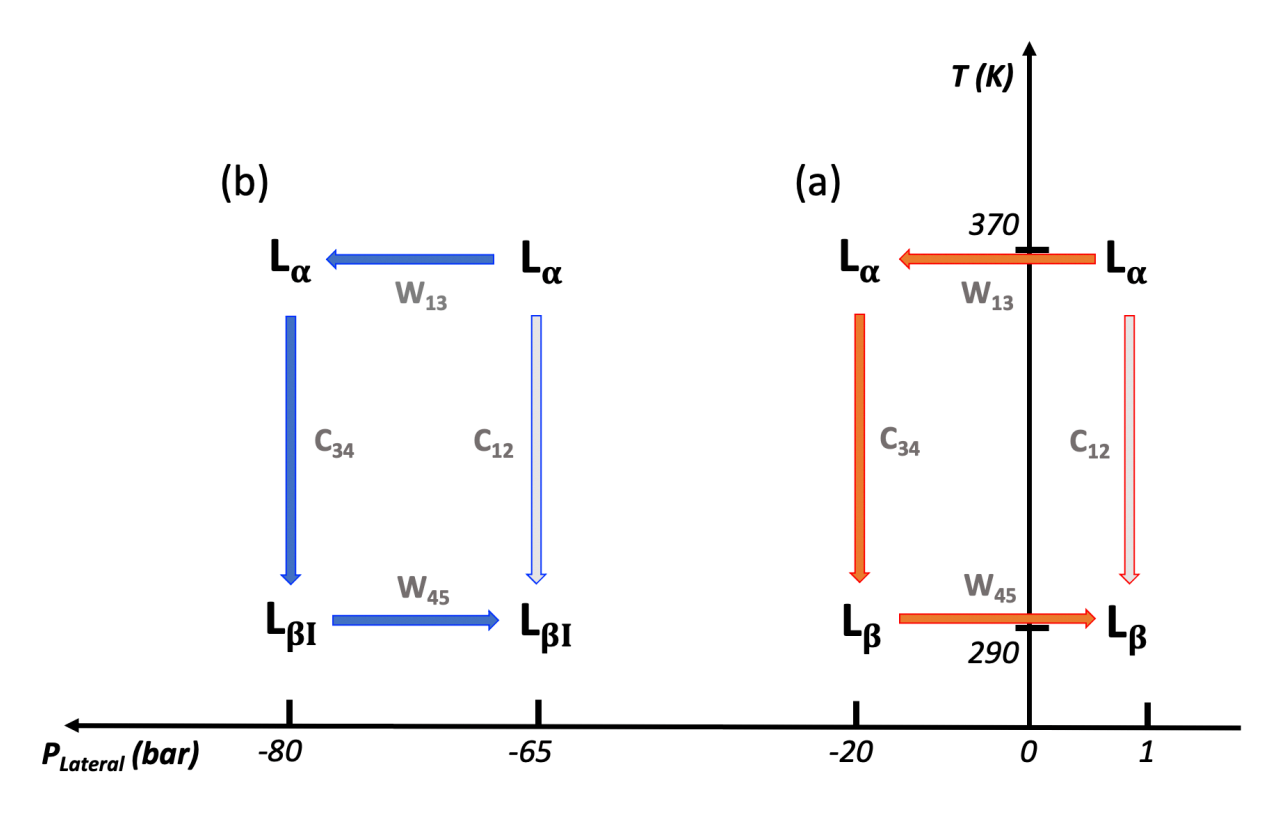


Figure 9. Thermodynamic cycles for (a) non-interdigitated bilayer, and (b) interdigitated bilayer. Solid and hollow arrows are different thermodynamic pathways connecting the same starting and final states.

$\Delta F = W_{45} + T_L \left[C_{34} - C_{12} + \frac{W_{13}}{T_H} \right]$ unit: kJ/mol					
System	$-C_{12}*T_L$	$W_{13} * T_L/T_H$	$C_{34} * T_L$	W_{45}	ΔF
$L_{\beta I}$ vs L_{β}	413.45	2.704	- 413.31	- 0.40	2.44
Cycle (a)	413.45	0.203	- 413.96	- 0.029	- 0.34
Cycle (b)	413.31	0.972	- 414.55	- 0.122	- 0.39

Table 1. Calculated values for C_{12} , W_{13} , C_{34} and W_{45} , each multiplied by temperature or temperature ratio used in calculating the free energy difference between the $L_{\beta I}$ and L_{β} phases and in the two constructed thermodynamic cycles.

Discussion

The major contribution of the excess free energy difference between the $L_{\beta I}$ phase and the L_{β} phase comes from the PV work (W_{10}) during stretching of the bilayer in the L_{α} phase. This is because the free energy change from the L_{α} to L_{β} phase and from the stretched L_{α} to $L_{\beta I}$ phase under negative lateral pressure almost cancel each other as shown in the first row of numerical values in Table 1. For the interdigitated bilayer to be the favored structure, the free energy of the $L_{\beta I}$ phase minus that of the L_{β} phase should be negative. This would require a smaller positive PV work during stretching (W_{10}) of the L_{α} phase and a larger free energy reduction upon turning the L_{α} phase into the $L_{\beta I}$ phase on cooling (C_{30}). The contribution of the entropy to the free energy difference can also be determined. The difference of internal energy is readily found from the simulation to be 3.05 kJ/mol. Using $\Delta F = \Delta U - T\Delta S$, the entropy difference of the $L_{\beta I}$ phase over that of the L_{β} phase is computed to be 2.2 J/(mol K) at 290 K. The higher entropy of the

interdigitated bilayer might be explained by the various ways the molecules from each leaflet can interpenetrate into the other leaflet in the bilayer.

5. Conclusion and Future Directions

Using MD simulations of bilayers of fatty alcohol and cationic surfactant, we induced the formation of an interdigitated L_{BI} bilayer from a non-interdigitated L_{B} phase, by 1) heating the L_{B} phase into an L_{α} phase, then 2) stretching the L_{α} bilayer using negative lateral pressure to induce interdigitation, and then 3) cooling to a lower temperature at which the L_{BI} phase formed. By thermodynamic integration, the free energy changes of each of these transformations were computed, although the third of these free energy changes were found to be more accurately determined by heating from the L_{BI} phase rather than the reverse. Both interpolation and extrapolation to zero heating rates were used in the free energy calculations to approximate the true equilibrium properties and two additional thermodynamic cycles designed to produce zero net free energy change were constructed to provide negative control, thus verifying the method. The free energy of the $L_{\beta I}$ phase was found to be 2.4 \pm 0.5 kJ/mol higher than that of L_{β} phase, which is consistent with the spontaneous formation of the L_{β} phase under atmospheric pressure in simulations of cooling from the L_{α} phase. To further improve the method, performing long simulations at different temperatures and using interpolation in between could be an alternative way to obtain the energy-temperature curve for thermodynamic integration and could be compared with the current approach. Using a different forcefield may also provide a better result although the forcefield gives a phase transition temperature of around 350-355 K, which is only 5-10 K higher than the experimental one. It would also be worthwhile to apply our method to other bilayer systems, especially those that experimentally show interdigitation to gain a better understanding

of the molecular requirements needed for interdigitation. We also note that there may be other solid-solid phase transitions in lamellar geometries for which lateral pressure might be used to determine relative phase stability.

Acknowledgement

We gratefully acknowledge Procter and Gamble Company for supporting this work financially. We acknowledge helpful discussions with Sumanth Jamadagni of P&G, and with Cyrus Safinya of University of California, Santa Barbara. Support was also provided by the National Science Foundation under grant CBET-1907517. Any opinions, findings, and conclusions or recommendations expressed in this material are those of the authors and do not necessarily reflect the views of NSF.

Supporting Information

Supporting Information includes figures showing the non-interdigitated and the interdigitated bilayer formed upon cooling at different lateral pressures, a comparison of results from the main paper with those from a smaller system and from a system with "homogenously" dispersed surfactant, and the results of thermodynamic integration of two thermodynamic cycles.

References

(1) Fukushima, S., Yamaguchi, M., & Harusawa, F. (1977). Effect of cetostearyl alcohol on stabilization of oil-in-water emulsion: II. Relation between crystal form of the alcohol and stability of the emulsion. *Journal of Colloid and Interface Science*, *59*(1), 159-165. https://doi.org/10.1016/0021-9797(77)90350-2

- (2) Barry, B. W., & Saunders, G. M. (1970). The Self-bodying action of the mixed emulsifier cetrimide/cetostearyl alcohol. *Journal of Colloid and Interface Science*, *34*(2), 300–315. https://doi.org/10.1016/0021-9797(70)90182-7
- (3) Laba, D. (1993). *Rheological properties of cosmetics and toiletries*. Routledge. https://doi.org/10.1201/9780203740651
- (4) Barry, B. W., & Eccleston, G. M. (1973). Influence of gel networks in controlling consistency of O/W emulsions stabilised by mixed emulsifiers. *Journal of Texture Studies*, 4(1), 53–81. https://doi.org/10.1111/j.1745-4603.1973.tb00654.x
- (5) Iwata, T. (2017). Lamellar gel network. In K. Sakamoto, R. Lochhead, H. Maibach & Y. Yamashita (Eds), *Cosmetic science and technology: Theoretical principles and applications* (pp. 415-447). Elsevier.
- (6) Datta, A., Tanmay, V. S., Tan, G. X., Reynolds, G. W., Jamadagni, S. N., & Larson, G. (2020) Characterizing the rheology, slip and velocity profiles of lamellar gel networks. *Journal of Rheology*, 64(4), 851-862. https://doi.org/10.1122/8.0000011
- (7) Larson, R. G. (1998). *The structure and rheology of complex fluids*. Oxford University Press.
- (8) Dubois, M., Zemb, T., Belloni, L., Delville, A. D. P., Levitz, P., & Setton, R. (1992).
 Osmotic pressure and salt exclusion in electrostatically swollen lamellar phases. *The Journal of Chemical Physics*, 96(3), 2278–2286.
 https://doi.org/10.1063/1.462078

(9) Debnath, A., Ayappa, K. G., Kumaran, V., & Maiti, P. K. (2009). The influence of bilayer composition on the gel to liquid crystalline transition. *The Journal of Physical Chemistry B*, 113(31), 10660–10668.
https://doi.org/10.1021/jp901551d

(10) Tiddy, G. J. T. (1980). Surfactant-water liquid crystal phases. *Physics Reports*, 57(1), 1–46.
 https://doi.org/10.1016/0370-1573(80)90041-1

(11) Quinn, P. J., Chapman, D., & Keith, A. D. (1980). The dynamics of membrane structure.

*Critical Reviews in Biochemistry, 8(1), 1–117.

https://doi.org/10.3109/10409238009105466

(12) Smith, E. A., & Dea, P. K. (2015). The interdigitated gel phase in mixtures of cationic and zwitterionic phospholipids. *Biophysical Chemistry*, 196, 86–91.
https://doi.org/10.1016/j.bpc.2014.10.003

(13) Barry, M. D., & Rowe, R. C. (1989). The characterisation by small-angle X-ray scattering of a pharmaceutical gel with a lamellar structure. *International Journal of Pharmaceutics*, 53(2), 139-143.

https://doi.org/10.1016/0378-5173(89)90237-8

(14) Eccleston, G. M., Behan-Martin, M. K., Jones, G. R., & Towns-Andrews, E. (2000). Synchrotron X-ray investigations into the lamellar gel phase formed in pharmaceutical creams prepared with cetrimide and fatty alcohols. *International Journal of Pharmaceutics*, 203(1-2), 127–139.

https://doi.org/10.1016/S0378-5173(00)00447-6

- (15) Naumann, C., Brumm, T., & Bayerl, T. M. (1992). Phase transition behavior of single phosphatidylcholine bilayers on a solid spherical support studied by DSC, NMR and FT-IR. *Biophysical Journal*, 63(5), 1314–1319.
 https://doi.org/10.1016/S0006-3495(92)81708-3
- (16) Shigematsu, T., Koshiyama, K., & Wada, S. (2018). Stretch-induced interdigitation of a phospholipid/cholesterol bilayer. *The Journal of Physical Chemistry B*, 122(9), 2556-2563. http://doi.org/10.1021/acs.jpcb.7b10633
- (17) Laner, M., Horta, B. A. C., & Hünenberger, P. H. (2014). Effect of the cosolutes trehalose and methanol on the equilibrium and phase-transition properties of glycerol-monopalmitate lipid bilayers investigated using molecular dynamics simulations. *European Biophysics Journal*, *43*(10–11), 517–544.

 https://doi.org/10.1007/s00249-014-0982-9
- (18) Laner, M., & Hünenberger, P. H. (2015). Effect of methanol on the phase-transition properties of glycerol-monopalmitate lipid bilayers investigated using molecular dynamics simulations: In quest of the biphasic effect. *Journal of Molecular Graphics and Modelling*, 55, 85–104.
- (19) Kranenburg, M., Vlaar, M., Smit, B. (2004). Simulating induced interdigitation in membranes. *Biophysical Journal*, 87(3), 1596-1605.
 https://doi.org/10.1529/biophysj.104.045005

https://doi.org/10.1016/j.jmgm.2014.10.017

(20) Lu, T., & Guo, H. (2018). Phase behavior of lipid bilayers: A dissipative particle dynamics simulation study. *Advanced Theory and Simulations*, 1, 1800013.

http://doi.org/10.1002/adts.201800013

- (21) Seo, S., Murata, M., Shinoda, W. (2020). Pivot role of interdigitation in interleaflet interactions: Implications from molecular dynamics simulations. *The Journal of Physical Chemistry Letters*, 11(13), 5171-5176.

 https://doi.org/10.1021/acs.jpclett.0c01317
- (22) Lunkad, R., Srivastava, A., & Debnath, A. (2017). Influence of water concentrations on the phase transformation of a model surfactant/co-surfactant/water system. *Chemical Physics*, 483–484, 103–111.
 https://doi.org/10.1016/j.chemphys.2016.11.014
- (23) de Oliveira, T. E., Leonforte, F., Nicolas-Morgantini, L., Fameau, A. L., Querleux, B., Thalmann, F., & Marques, C. M. (2020). Fluid bilayer phase in aqueous mixtures of fatty alcohol and cationic surfactant. *Physical Review Research*, 2(1), 013075.

 https://doi.org/10.1103/PhysRevResearch.2.013075
- (24) Jorgensen, W. L., Maxwell, D. S., & Tirado-Rives, J. (1996). Development and testing of the OPLS all-atom force field on conformational energetics and properties of organic liquids. *Journal of the America Chemical Society*, 118, 11225–11236. https://doi.org/10.1021/ja9621760
- (25) Siu, S. W. I., Pluhackova, K., Böckmann, R. A. (2012). Optimization of the OPLS-AA force field for long hydrocarbons. *Journal of Chemical Theories and Computation*, 8(4), 1459-1470.
 https://doi.org/10.1021/ct200908r
- (26) Zangi, R. (2018). Refinement of the OPLSAA Force-Field for Liquid Alcohols. ACS Omega, 3(12), 18089–18099.
 https://doi.org/10.1021/acsomega.8b03132

- (27) Bussi, G., Donadio, D., Parrinello, M. (2007). Canonical sampling through velocity rescaling. *The Journal of Chemical Physics*, *126*(1), 014101.

 https://doi.org/10.1063/1.2408420
- (28) Parrinello, R., Rahman, A. (1981). Polymorphic transitions in single crystals: A new molecular dynamics method. *Journal of Applied Physics*, 52(12), 7182. https://doi.org/10.1063/1.328693
- (29) Darton, T., York, D., Pedersen, L. (1993). Particle mesh Ewald: An N log(N) method for Ewald sums in large systems. *The Journal of Chemical Physics*, 98(12), 10089.
 https://doi.org/10.1063/1.464397
- (30) Berendsen, H. J. C., van der Spoel, D., & van Drunen, R. (1995). GROMACS: A message-passing parallel molecular dynamics implementation. *Computer Physics Communications*, 91(1-3), 43–56.

 https://doi.org/10.1016/0010-4655(95)00042-E
- (31) Abraham, M., Murtola, T., Schulz, R., Páll, S., Smith, J. C., Hess, B., Lindaul, E. (2015).
 GROMACS: High performance molecular simulations through multi-level parallelism from laptops to supercomputers. *SoftwareX*, 1(2), 19-25.
 https://doi.org/10.1016/j.softx.2015.06.001

TOC Graphic

